Liquid Crystals
Publication details, including instructions for authors and subscription information:
http://www.informaworld.com/smpp/title~content=t713926090

A SAXS study of flow alignment of thermotropic liquid crystal mixtures

V. Castelletto[a]; A. M. Squires[a]; I. W. Hamley[a]; J. Stasiak[b]; G. D. Moggridge[b]
[a] Department of Chemistry, University of Reading, Reading, UK [b] Department of Chemical Engineering and Biotechnology, University of Cambridge, Pembroke Street, Cambridge, UK

To cite this Article Castelletto, V. , Squires, A. M. , Hamley, I. W. , Stasiak, J. and Moggridge, G. D.(2009) 'A SAXS study of flow alignment of thermotropic liquid crystal mixtures', Liquid Crystals, 36: 4, 435 — 442
To link to this Article: DOI: 10.1080/02678290902928542
URL: http://dx.doi.org/10.1080/02678290902928542

Liquid Crystals,
Vol. 36, No. 4, April 2009, 435–442

Taylor & Francis
Taylor & Francis Group

A SAXS study of flow alignment of thermotropic liquid crystal mixtures

V. Castelletto[a]*, A.M. Squires[a], I.W. Hamley[a], J. Stasiak[b] and G.D. Moggridge[b]

[a]*Department of Chemistry, University of Reading, Reading RG6 6AD, UK;* [b]*Department of Chemical Engineering and Biotechnology, University of Cambridge, Pembroke Street, Cambridge, CB2 3RA, UK*

(Received 20 February 2009; final form 27 March 2009)

We report on the capillary flow behaviour of thermotropic liquid crystal mixtures containing 4-*n*-octyl-4′-cyanobiphenyl (8CB) and 4-*n*-pentyl-4′-cyanobiphenyl (5CB). The liquid crystal mixtures are studied in the Nematic (N) and Smectic (S_A) phases at room temperature. Polarised optical microscopy (POM), rheology and simultaneous X-ray diffraction (XRD)/capillary flow experiments are performed to characterise the system.

Polarised optical microscopy reveals a dramatic change in optical texture when the 5CB content is increased from 20 to 30% in the mixtures. X-ray diffraction results show that the system goes through a S_A–N phase transition, such that the mixtures are smectic for 10–20% 5CB and nematic for 30–90% 5CB. Smectic mixtures flow with the layers aligned along the flow direction (mesogens perpendicular to flow) while nematic mixtures flow with the mesogens aligned in the flow direction. Simultaneous XRD/shear flow experiments show that the S_A–N transition is independent of the flow rate in the range 1–6 ml min^{-1}.

The correlation length of the liquid crystal order decreases with increasing 5CB content. Rheology is used to prove that the correlation length behaviour is related to a reduction in the viscosity of the mixture.

Keywords: X-ray diffraction; nematic; smectic, mixtures; flow alignment

1. Introduction

Thermotropic liquid crystals are model soft materials that exhibit responsiveness to external fields. Their use in optoelectronic displays relies both on their response to electromagnetic fields and their alignment at surfaces (*1*).

In previous work, the Hamley group investigated the capillary flow behaviour of the thermotropic liquid crystal 4-*n*-octyl-4′-cyanobiphenyl (8CB) which exhibits both smectic (S_A) and nematic (N) phases (*2*). Samples were cooled from the isotropic phase to erase prior orientation and studied by small angle X-ray scattering (SAXS). Upon cooling through the N phase a transition from alignment of mesogens along the flow direction to alignment of pre-transitional layers along the flow direction (mesogens perpendicular to flow) was observed. The transition was centred on a temperature at which the Leslie viscosity coefficient α_3 changes sign. The configuration with layers aligned along the flow direction was also observed in the smectic phase. The transition in the N phase on cooling has previously been ascribed to an aligning–non-aligning or tumbling transition. At high flow rates, there was evidence for tumbling around an average alignment of layers along the flow direction. At lower flow rates this orientation is more clearly defined. The alignment of 8CB under shear flow was first investigated by Safinya *et al.* (*3*) via SAXS, using a Couette geometry, probing the orientation in the (**v**, **e**) and (∇**v**, **e**) planes. Here, **v** is the flow direction, ∇**v** denotes the shear gradient direction and **e** is the neutral direction. With reference to Scheme 1, they observed the 'b' state in the N phase at high temperature close to the isotropic state, a region of coexisting 'a' and 'b' orientations at intermediate temperature, and the 'a' orientation at lower temperature, approaching the N–S_A transition temperature T_{NA}. Subtle differences in the 'a' state were distinguished based on the orientation of diffuse scattering features. Later, Panizza *et al.* correlated the viscosity of 8CB in the smectic phase under Couette shear with changes in the orientation state as probed by SAXS (*4*) but did not examine the N phase.

The cyanobiphenyl liquid crystals (*n*CB series) are particularly important for applications in liquid crystal displays. In commercial applications, eutectic mixtures of these materials are used (*5*) (sometimes containing cyanoterphenyls), since the operating temperature range in the N phase can be extended compared with single-component systems (*6*). Among the *n*CB series, 4-*n*-pentyl-4′-cyanobiphenyl (5CB) is the lowest homologue to exhibit an enantiotropic N phase, and 4-*n*-octyl-4′-cyanobiphenyl (8CB) is the first member of the series to show a S_A phase (which is stable at temperatures below the N phase region). By mixing these two liquid crystals, the nematic phase region can be adjusted. Since the elastic and flow properties of liquid crystals depend on how far the system is from the smectic phase, mixing liquid crystals offers the possibility to access interesting flow behaviours. Note that for higher homologues such as 4-*n*-decyl-4′-cyanobiphenyl (10CB), the N phase is absent. In mixtures of 10CB with lower homologues, tricritical points are therefore

*Corresponding author. Email: v.castelletto@reading.ac.uk

ISSN 0267-8292 print/ISSN 1366-5855 online

DOI: 10.1080/02678290902928542
http://www.informaworld.com

encountered (*7*). The bend elastic constant and rotational constant diverge at the tricritical point (*8*). In the present work, we avoid the tricritical point in a mixture of *n*CB liquid crystals (8CB and 5CB) both forming N phases as pure compounds.

In this work, we perform simultaneous capillary flow/SAXS experiments on 5CB/8CB mixtures. This investigation represents a step further in our work on shear flow experiments of 8CB. We are aware of only one prior report on 5CB/8CB mixtures, which is a study of the optical behaviour and related properties of the binary mixtures as a function of their molar composition (*9*). We are not aware of prior X-ray scattering studies on the structure of 5CB/8CB mixtures and capillary flow behaviour. In this work, the capillary flow behaviour of the mixtures will be studied using a flow cell device developed in our laboratory, together with an in-house X-ray scattering setup. The morphology of the mixtures will be characterised in terms of their rheological properties, shear flow alignment and optical texture.

2. Experimental section

2.1 Materials

The samples of 5CB and 8CB were purchased from Kingston Chemicals (Hull, UK) and used without further purification. The pure components present different phases (K: crystalline, N: nematic, S_A: smectic A, I: isotropic), depending on the temperature. The sequence of phase transitions for the pure components is well known and obeys the following order (*3, 10, 11*):

$$5CB : K \rightarrow 24^{\circ}C \rightarrow N \rightarrow 35^{\circ}C \rightarrow I$$

$$8CB : K \rightarrow 21.5^{\circ}C \rightarrow S_A \rightarrow 33.5^{\circ}C \rightarrow N \rightarrow 40.5^{\circ}C \rightarrow I.$$

5CB/8CB mixtures were prepared by mixing the individual components at 50°C, to ensure that both components were in the isotropic phase according to the phase sequence above. Liquid crystal mixtures were prepared with a composition of Δ = 10–90 wt% 5CB. All the experiments described in this paper were performed at room temperature (20°C).

2.2 Shear flow cell

We constructed a capillary flow device, similar to that developed by Bernal and Fankuchen (*12*), for use in time-resolved scattering studies of flow-induced alignment. Details of this machine have been given elsewhere (*13*). Briefly, the central part of the capillary flow device is a computer-controlled peristaltic pump that allows controlled volume and time dispensing. The flow rate is recorded and the unit is interfaced to a PC for acquisition of flow rate data. We used borosilicate capillaries with D = 1 mm internal diameter and 0.01 mm wall thickness. The measured flow rates were in the range Q = 1–6 ml min^{-1}. These correspond to Newtonian shear rates at the wall of $\dot{\gamma} = 32Q/\pi R^3$ = 170 s^{-1} to 1020 s^{-1}. The actual flow rate will differ for non-Newtonian fluids, and for this reason we quote flow rates Q.

2.3 Polarised optical microscopy (POM)

Images were obtained with an Olympus BX41 polarised microscope by placing the sample between crossed polarisers. Samples were placed between a glass slide and a coverslip before capturing the images with a Canon G2 digital camera.

2.4 X-ray diffraction (XRD)

Experiments were carried out using the four axis goniometer of a RAXIS IV++ X-ray diffractometer (Rigaku) equipped with a rotating anode generator. The XRD data was collected using a Saturn 992 CCD camera. The sample-detector distance was 90 mm for all the experiments.

The X-ray wavelength was λ = 1.54 Å. The wavenumber scale ($q = 4\pi \sin\theta/\lambda$ where 2θ is the scattering angle) was geometrically calculated using the size of each pixel in the detector screen (0.0898 mm) and the sample–detector distance.

The capillary flow cell was positioned with the flow direction $\mathbf{v}$ parallel to the horizontal (x-axis) in the 2D detector plane. A circular X-ray beam collimation was used, such that the beam profile had a 0.5 mm diameter when hitting the sample.

In order to analyse the data from the two-dimensional detector, the 2D XRD data from the flow cell was reduced by azimuthal integration (I_ϕ; ϕ: azimuthal angle) centred on the scattering ring of interest. The radial intensity (I_r) was obtained by radially integrating the 2D profile over the range $0 \leq \phi \leq 180^{\circ}$.

2.5 Rheology

Rheological properties were determined using a controlled stress TA Instruments AR-2000 rheometer (TA Instruments). The viscosity of the samples was measured performing controlled stress experiments with a cone-and-plate geometry (cone radius = 20 mm; cone angle = 1°).

3. Results and discussion

A POM study of the mixtures was undertaken before the simultaneous XRD/capillary flow experiments, in

order to investigate gross morphological changes in the texture of different phases.

Mixtures of 5CB and 8CB containing 0–100 wt% 5CB were observed by POM. Some representative results are shown in Figure 1. Mixtures containing Δ = 0–20 wt% 5CB were not birefringent when observed through crossed polarisers, in contrast to mixtures with Δ = 30–100 wt% 5CB, which were strongly birefringent when observed through crossed polarisers (Figure 1).

Calorimetric and optical experiments on 5CB/8CB mixtures have been reported in the literature (*9*). That work provided the orientational order parameter of the phase and the hard core length-to-breath ratio of the molecules for mixtures containing 10–90 wt% 5CB at 20°C (*9*). In particular, the existence of a N phase was identified, for mixtures containing 30–90 wt% 5CB at 20°C (*9*). However, no information was given regarding the structural features of mixtures containing 10–20 wt% 5CB at 20°C, even if the determination of an order parameter for these compositions indicates a liquid crystal order (*9*).

Our POM results (Figure 1) show a dramatic change in optical texture, associated with a change in liquid crystal order, when the mixture composition changes from 10–20 wt% 5CB to 30–90 wt% 5CB. According to the paragraph above, mixtures with 30–90 wt% 5CB are in the N phase at room temperature, which is the same phase observed for the pure 5CB at room temperature. Enriching the content of a particular component drives the liquid crystal order of the mixture towards the liquid crystal order of that particular component. In keeping with that idea, mixtures with highest 8CB content (i.e. 10–20 wt% 5CB) should exhibit S_A order, since the pure 8CB forms S_A phase at room temperature.

It is, therefore, expected that the capillary flow behaviour of mixtures with 10–20 wt% 5CB will be different from that corresponding to mixtures containing 30–90 wt% 5CB. Simultaneous XRD/capillary flow experiments were done for mixtures with 10–90 wt% 5CB. For each sample the flow behaviour was studied for flow rates in the range Q = (0.1–6) ml min^{-1}. In order to investigate the influence of flow on alignment, the samples were first heated into the isotropic phase (T = 50°C).

In good agreement with the POM results discussed above, the overall features of the XRD patterns obtained for the mixtures oriented under capillary flow could be grouped in two different sets, comprising mixtures with 10–20 wt% 5CB and 30–90 wt% 5CB. The general features of the XRD patterns did not change as a function of the flow rate within the range Q = 0.1–6 ml min^{-1}.

Figure 2 shows the XRD patterns obtained for mixtures containing 10 and 90 wt% 5CB under flow (Q = 6 ml min^{-1}) as representative examples for the flow alignment obtained for 10–20 wt% 5CB and 30–90 wt% 5CB, respectively. Flow XRD patterns for mixtures containing 10–90 wt% 5CB, were characterised by two oriented scattering rings, one at low scattering angles (ring 1 in Figure 2) and another at high scattering angles (ring 2 in Figure 2). Ring 2 remained broad for 10–90 wt% 5CB, while ring 1 was sharp for 10–20 wt% 5CB and broad for 30–90 wt% 5CB. In addition to the two scattering rings, samples containing 60–90 wt% 5CB presented an oriented diffuse scattering at angles slightly higher than those measured for the inner sharp scattering ring (feature 3 in Figure 2(b)). Similar diffuse scattering has been previously reported for 7CB at 27°C (being absent for 5CB samples at similar temperatures) (*11*).

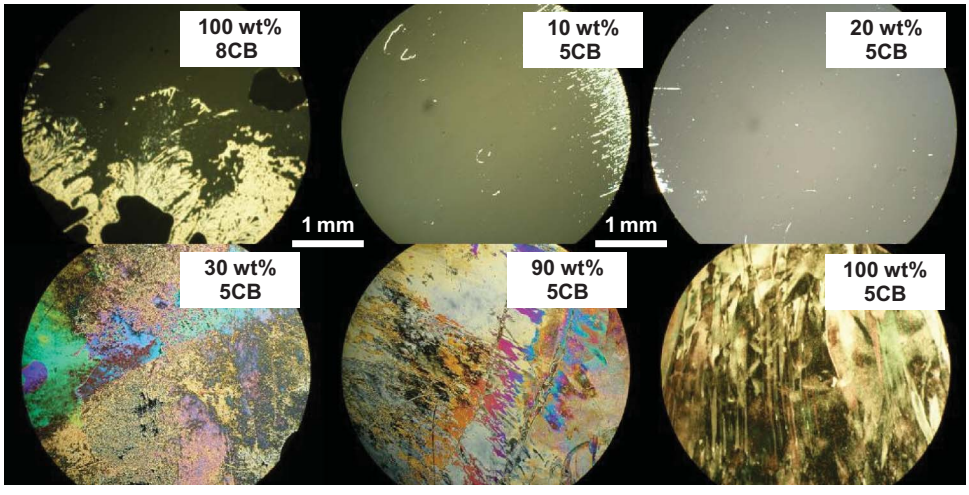

Figure 1. Polarised optical microscopy corresponding to 5CB/8CB mixtures and pure 5CB and 8CB samples.

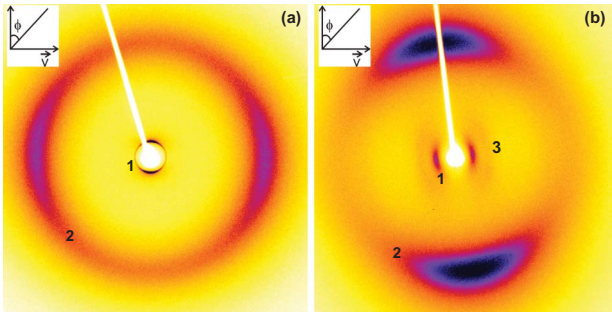

Figure 2. X-ray diffraction results obtained for 5CB/8CB mixtures containing (a) 10 and (b) 90 wt% 5CB. The inset shows the azimuthal coordinates and the flow direction with respect to the 2D image on the detector. All the data has been obtained at $Q = 6$ ml min^{-1}.

We observed a clear transition in flow orientation when the mixture composition changes from 10–20 wt% 5CB to 30–90 wt% 5CB. According to Scheme 1, the sample flows in the 'c' orientation when the mesogens flow perpendicular to the flow direction and the monodomains flow parallel to the flow direction. This configuration corresponds to the azimuthal intensity of peak 1 and peak 2 centred on the meridian and the equator of the XRD pattern, respectively. The 'b' orientation is attained when the mesogens flow parallel to the flow direction. This configuration leads to the azimuthal intensity within ring 1 and ring 2 centred on the equator and the meridian of the XRD pattern, respectively. It can be concluded from Figure 2 that the mixtures flow align in the 'c' configuration for 10–20 wt% 5CB and close to the 'b' configuration for 30–90 wt% 5CB, although there is some tilt in the SAXS pattern (ride infra).

In a previous study, involving simultaneous SAXS/flow behaviour for 8CB (*2*), we observed that the liquid crystal flow aligns in the 'c' configuration within the S_A phase. Those experiments only monitored ring 1 in Figure 2, and they show that although it is relatively broad and smooth in the N phase, it becomes intense and sharp in the S_A phase. Bringing together the information on peak orientation, it is possible to affirm that mixtures with 10–20 wt% 5CB are in the S_A phase, as discussed before in relation to the POM results (Figure 1).

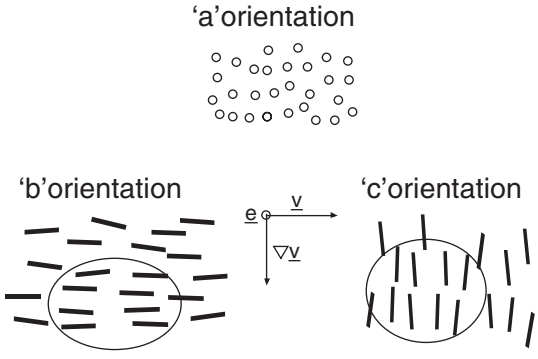

Scheme 1. Schematic of the three orientations of the nematic phase under flow. Regions of smectic fluctuations are highlighted.

At this point it is worth underlining that the N phase flow aligns in the 'b' configuration throughout the Δ = 30–90 wt% 5CB. In this sense, our experiments did not prove the existence of pre-transitional smectic fluctuations close to the S_A–N phase transition, represented by N domains flow aligned in a 'c' configuration (*2*). Usually, the existence of pre-transitional smectic fluctuations in the N phase is proved by an increase in the intensity of peak 1 as the S_A phase is approached by cooling from above. Indeed, pre-transitional smectic fluctuations in the N phase may not be observed for 8CB/5CB mixtures studied in our work, because experiments were undertaken at room temperature and the S_A–N transition is driven by changes in the sample composition.

The azimuthal profiles of the patterns in Figure 2 are shown in Figure 3. A Gausssian fitting of the azimuthal scattering peaks was used to determine the parameters ϕ_1, ϕ_2 and $\Delta_{\phi 1}$ (Figure 3).

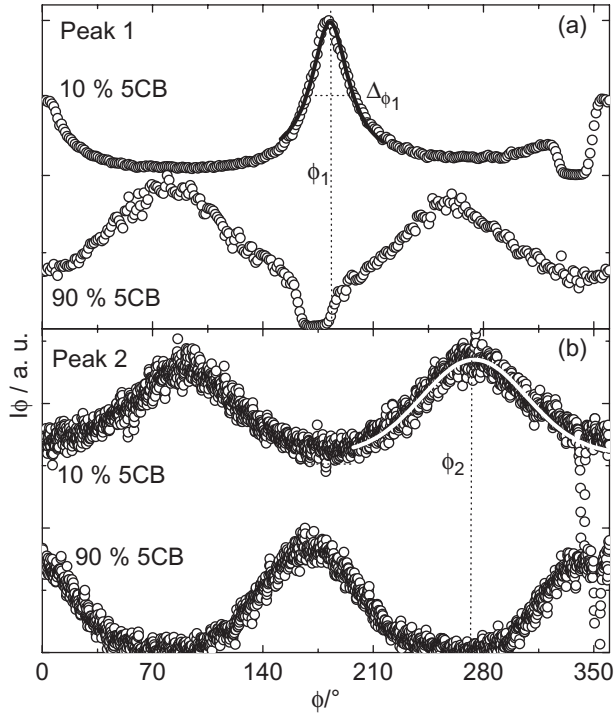

Figure 3. Azimuthal intensity for (a) peak 1 and (b) peak 2 corresponding to the 10 and 90 wt% 5CB mixture X-ray diffraction images shown in Figure 2. The curves have been shifted by an arbitrary factor to enable visualisation of the data. The full white and black lines are Gaussian fits to the peaks, used to determine ϕ_1, ϕ_2 and $\Delta_{\phi 1}$. All the data has been obtained at $Q = 6$ ml min^{-1}.

The scattering ring 1 (Figure 2) arises from the liquid crystal (smectic or nematic) ordering along the director (*2, 11*). Therefore, ϕ_1 gives the flow orientation of the monodomains, while $\Delta_{\phi 1}$ is a measure of the orientational correlation (mosaicity) of the monodomains. The scattering ring 2 (Figure 2) is associated to the spacing between mesogens perpendicular to the long axis of the mesogens (*2, 11*). In this way, ϕ_2 provides the flow orientation of the mesogens.

The azimuthal intensity of peak 2 is used to calculate the order parameter F of the system, given by the Herman's orientation parameter (*14*):

$$F = \left(3 < \cos^2 \phi > - 1\right)/2 \qquad (1)$$

where $<\cos^2\phi>$ is given by:

$$< \cos^2 \phi > = \frac{\int_0^{\pi} I(\theta, \phi) \cos^2 \phi \sin \phi d\phi}{\int_0^{\pi} I(\theta, \phi) \sin \phi d\phi} \qquad (2)$$

where $I(\theta,\phi)$ represents the scattered intensity at a given polar (θ) and azimuthal (ϕ) angle, measured from the assigned zero. The relations $0 < F < 1$ or $-0.5 < F < 0$ are valid for rod-like objects aligned along or perpendicular to the flow direction respectively. The particular case $F = 1$ corresponds to rod-like objects perfectly aligned along the flow direction while $F = -0.5$ describes rod-like objects perfectly aligned perpendicular to the flow direction. Finally, $F = 0$ describes a system of rod-like objects randomly aligned under flow.

The dependence of ϕ_1, ϕ_2, $\Delta_{\phi 1}$ and F with the composition of the liquid crystal mixtures is shown in Figure 4. In particular, the results in Figure 4 show that the flow behaviour does not change for flow rates Q = 1–6 ml min^{-1}.

Figure 4(a) and (b) show the dependence of the sample orientation under flow. The fingerprint of a sample flowing in the 'c' or in the 'b' configuration (Scheme 1) is given by Peaks 1, 2 with ($\phi_1 = 180°$, $\phi_2 = 270°$) or ($\phi_1 = 90°$, $\phi_2 = 180°$), respectively.

According to the paragraph above, Figure 4(a) and (b) show that the sample flows in the 'c' configuration within the S_A phase (Δ = 10–20 wt% 5CB) and in the 'b' configuration within the N phase (Δ = 40–90 wt% 5CB). A non-aligning (tumbling) flow behaviour is observed in the N phase for 70–90 wt% 5CB, although the 'b' orientation is not completely lost. The tumbling behaviour is denoted by a progressive shift in ϕ_2 from 180° to 172° for Δ increasing from 70 to 90 wt% 5CB (Figure 4(b)) (*2*).

Tumbling behaviour is characteristic of the flow alignment of rod-like nematic liquid crystals within a range of temperatures and viscosities, which varies depending on the molecular liquid crystal structure (*15*). For example, we previously found that the onset of non-aligning behaviour for 8CB corresponds to 38°C (*2*), in good agreement with the predicted temperature of 38.36°C (*15*). The progressive tumbling behaviour shown in Figure 4(b) suggests that the onset temperature for tumbling behaviour decreases upon increasing the content of 5CB within the N phase of 5CB/8CB mixtures.

The mosaicity is a measure of the number of monodomains in the sample which have a correlated orientation. Figure 4(c) shows that the mosaicity of the liquid crystal domains increases upon adding 5CB to the mixtures. Simultaneously the dependence of $\Delta_{\phi 1}$ is discontinuous through the S_A–N phase transition of the system (which lies in the range Δ = 20–30 wt% 5CB). In

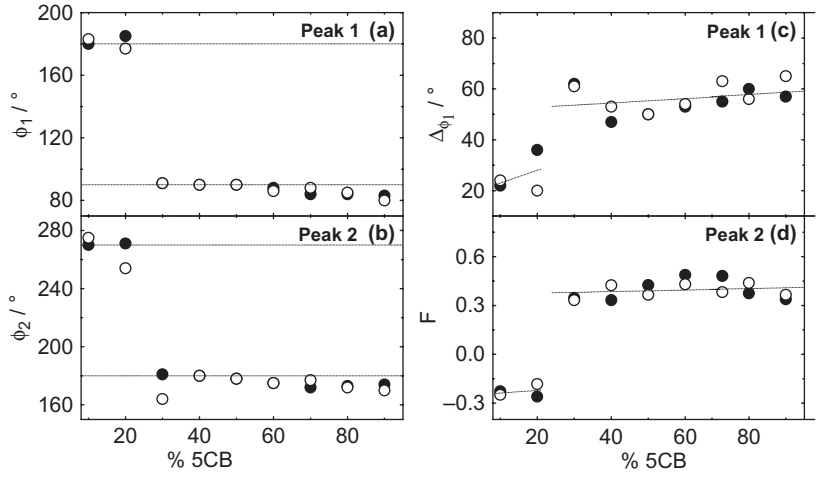

Figure 4. Dependence of the maximums in (a) and (b) the azimuthal intensity ($\phi_{1,2}$), (c) mosaicity ($\Delta_{\phi 1}$) and (d) order parameter (F) with the mixture composition. The broken lines are a guide to the eyes. Data are shown corresponding to Q = (●) 1 or (○) 6 ml min^{-1}.

the S_A phase the monodomains adopt a 'c' configuration, oriented perpendicular to the flow direction, while in the N phase the sample flows in the 'b' orientation, with mesogens oriented parallel to the flow direction. The discontinuity in $\Delta_{\phi 1}$ as a function of the mixture composition denotes the change in flow orientation of the liquid crystal phase. Values of $\Delta_{\phi 1}$ are higher in the N phase than in the S_A phase (Figure 4(c)), due to a greater spread of orientations between monodomains.

Figure 4(d) contains the orientation factor F for the liquid crystal mixtures as a function of the mixture composition. In good agreement with data in Figure 4(c), the order parameter presents a discontinuity through the S_A–N phase transition. According to Figure 4(d), $F \sim -0.2$ in the S_A phase (when the system adopts the 'c' configuration) while $F \sim 0.4$ in the N phase (when the system flows in the 'b' configuration). This result provides a picture of partial shear flow alignment both in the S_A and the N phases, in good agreement with the 'half moon profiles' of the XRD rings (Figure 1).

The radial intensity profile of the patterns in Figure 2 are shown in Figure 5. By measuring the position of the peak 1 maximum in the radial intensity profile, q_1, the parameter $d_1 = 2\pi/q_1$ can be calculated. Similarly, the parameter $d_2 = 2\pi/q_2$ is calculated from the position of the peak 2, q_2. d_1 corresponds to the 'molecular length' or 'spacing', while d_2 corresponds to the lateral distance between molecules perpendicular to the long axis of the mesogens (*2*, *11*). The dependence of d_1 and d_2 on the composition of the 5CB/8CB mixtures is shown in Figure 6.

The scattering peaks 1 and 2 in the radial intensity profile could be modelled with a Lorentzian:

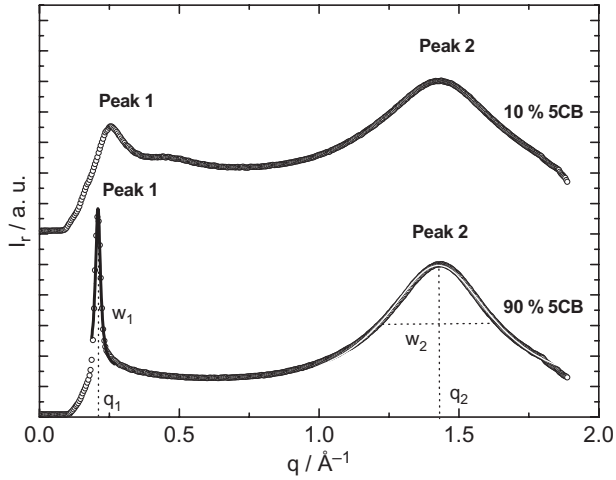

Figure 5. Radial intensity corresponding to the 10 and 90 wt% 5CB/8CB mixtures X-ray diffraction images shown in Figure 2. The curves have been shifted by an arbitrary factor in order to enable the visualisation of the data. The full white and black lines are a fit to the peak, showing q_1, q_2, Δ_{q1} and Δ_{q2}. All the data have been obtained at $Q = 6$ ml min^{-1}.

$$I(q) = BG + \frac{A\Delta_q}{2\pi(q - q_o)^2 + \Delta_{q^2}} \qquad (3)$$

where BG is the incoherent background, A is proportional to the intensity and Δ_q is the full width at half maximum of the Lorentzian.

In general, one may relate the half width of the diffraction peak Δ_q to a correlation length Δ_d by $2\pi/\Delta_q = X\Delta_d$ where X is a number of order unity which

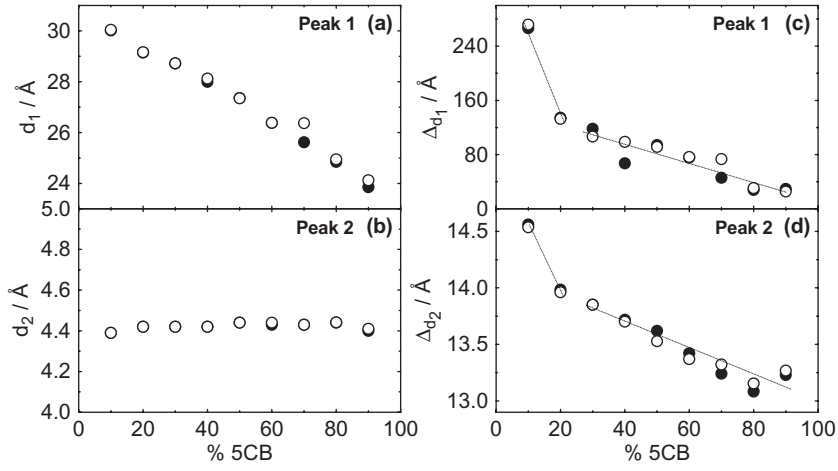

Figure 6. Dependence of (a) average molecular length (d_1), (b) average distance between mesogens (d_2) and (c) and (d) and correlation lengths ($\Delta_{d1,2}$) with the mixture composition for peak 1 and peak 2. The broken lines are a guide to the eyes. Data are shown corresponding to Q = (●) 1 or (○) 6 ml min^{-1}.

depends on the model used to define Δ_d (*16*). We do not require the absolute value of Δ_d and therefore we will quantify the extent of order by using $X = 1$ to define the correlation length. The dependence of Δ_{d1} and Δ_{d2} (associated to peaks 1 and 2, respectively) on the composition of the 5CB/8CB mixtures is shown in Figure 6 for Q = 1–6 ml min^{-1}.

Figure 6 shows, similarly to Figure 4, that the spacings from the XRD patterns are not affected by the flow rate within the range studied in this work. In addition, Figure 6(a) and (b) show that $d_{1,2}$ vary continuously with the mixture composition, since they are related to the geometrical dimensions of the molecule. 5CB and 8CB molecules have the same width, while the length of the extended molecule is shorter for 5CB than for 8CB. Therefore, while d_2 is expected to remain constant through the S_A–N transition, d_1 is expected to decrease continuously upon increasing the content of 5CB in the mixture. In contrast, the dependence of $\Delta_{d1,2}$ with the mixture composition is discontinuous through the N–S_A phase transition (Figure 6 (c) and (d)), because $\Delta_{d1,2}$ are constrained by the structural order of the system which is discontinuous through the N–S_A phase transition.

The molecular length for the sample with 10 wt% 5CB (Figure 6(a)) is very close to the S_A spacing reported for 8CB at low temperature, $d_1 \sim$ 32 Å (*2*, *17*, *18*). Similarly, the molecular length for the sample with 90 wt% 5CB (Figure 6(a)) is close to spacing for the N phase measured for 5CB at 20°C, $d_1 \sim$ 23.5 Å (results not shown). The spacing d_1 decreases continuously from 30 to 24 Å, upon increasing the 5CB content in the mixtures (Figure 6(a)).

The average side-to-side intermolecular spacing in Figure 6(b) is ~ 4.5 Å. As reported in the literature (*11*), this spacing corresponds approximately to the average width of the molecule and is certainly smaller than the diameter of the freely oriented molecule (~ 6.5 Å). As mentioned above, the side-to-side intermolecular distance in these materials is not expected to change with the mixture composition, remaining indeed constant even throughout the N and I phase for the 5CB (*11*).

Both the correlation lengths of the molecular order and the liquid crystal order decrease with increasing 5CB content in the mixtures (Figure 6(c) and (d)). The decrease in the correlation length is certainly correlated to the progressive decrease in the mixture viscosity (η), which can be observed by the naked eye, upon increasing the 5CB content in 5CB/8CB mixtures.

The mixture viscosity was measured. Figure 7 shows the results obtained for Δ = 10–90 wt% 5CB, within the interval of shear rates measured by capillary flow ($\dot{\gamma} = 32Q/\pi R^3$ = 170 s^{-1} to 1020 s^{-1}). The mixture for Δ = 10 wt% 5CB shows a shear thinning behaviour,

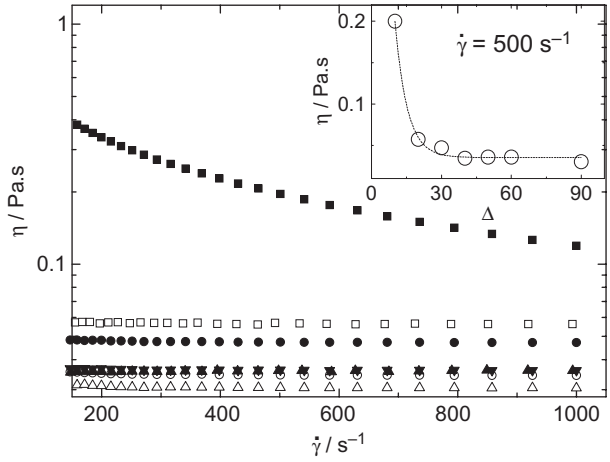

Figure 7. Viscosity of mixtures containing Δ = (■) 10, (□) 20, (●) 30, (○) 40, (▼) 50, (▲) 60 and (△) 90 wt% 5CB. The inset shows the dependence of the viscosity with Δ for $\dot{\gamma} = 500 s^{-1}$.

while the viscosity of the mixtures is independent of the shear rate for Δ = 20–90 wt% 5CB.

The shear thinning behaviour for 10 wt% 5CB (Figure 7) is probably associated with structural changes in the mixture induced by the shear flow. However, these hypothetical dynamic structural changes did not influence the shear flow orientation of the mixture for Q = 1–6 ml min^{-1}.

The inset in Figure 7 clearly shows that the viscosity of the mixtures decreases upon increasing the content of 5CB. The enhanced fluidity of the system for higher Δ is a macroscopic phenomena arising from the microscopic reduction in Δ_d measured upon increasing the 5CB content in the mixture (Figures 6(c) and (d)).

4. Conclusions

In this work we performed POM, simultaneous XRD/capillary flow and rheology experiments on mixtures of 5CB/8CB liquid crystal at room temperature. Our results showed the formation of a S_A liquid crystal phase for mixtures containing Δ = 10–20 wt% 5CB and a N phase for Δ = 30–90 wt% 5CB. Shear flow experiments also show that the results are independent of the flow rate for Q = 1–6 ml min^{-1}.

The S_A phase in mixtures rich in 8CB adopted a 'c' configuration under flow while the mixtures in the N phase flow aligned in the 'b' configuration. Nematic mixtures with higher content of 5CB showed a weak tumbling behaviour. The order parameter of the mixtures exhibits a discontinuity through the S_A–N phase transition, in agreement with a change in flow orientation of the sample.

The positional correlation length decreases with increasing 5CB content. Such an increase in structural disorder is correlated with a reduction in the viscosity of the mixture, as expected for a system with progressively reduced spatial constraints. Viscosity measurements on the mixtures show a shear thinning behaviour for Δ = 10 wt% 5CB. However, possible dynamic structural changes associated with the shear thinning behaviour did not influence the flow alignment of the mixture.

Pre-transitional smectic fluctuations have been observed in simultaneous SAXS/flow experiments performed through the S_A–N phase transition of 8CB (*2, 3*). The S_A–N phase transition was accessed on cooling in the 8CB system. In contrast, here the S_A–N phase transition is achieved through sample composition changes in 5CB/8CB mixtures at a constant temperature. The phase transition in 5CB/8CB mixtures takes place without the formation of pre-transitional smectic fluctuations in the system, and it might be defined as a first order transition.

Acknowledgements

VC thanks Mr. Nick Spencer (Biocentre, University of Reading) for assistance with XRD experiments, and Gemma Newby for assistance during rheology experiments.

References

(1) Clark, M.G.; Harrison, K.J.; Raynes, E.P. *Phys. Techn.* **1980**, *11*, 232–240.
(2) Hamley, I.W.; Castelletto, V.; Parras, P. *Phys. Rev. E* **2006**, *74*, 020701(R).
(3) Safinya, C.R.; Sirota, E.B.; Plano, R.J. *Phys. Rev. Lett.* **1991**, *66*, 1986–1989.
(4) Panizza, P.; Archambault, P.; Roux, D. *J. Phys. France II* **1995**, *5*, 303–311.
(5) Hulme, D.S.; Raynes, E.P.; Harrison, K.J. *J. Chem. Soc. Chem. Commun.* **1974**, 1974, 98–99.
(6) Collings, P.J.; Hird, M., *Introduction to Liquid Crystals. Chemistry and Physics*. Taylor and Francis: London, 1997.
(7) de Gennes, P.G.; Prost, J., *The Physics of Liquid Crystals*. 2nd Ed.; Oxford University Press: Oxford, 1993.
(8) Dasgupta, B.R.; Tee, S.Y.; Crocker, J.C.; Frisken, B.J.; Weitz, D.A. *Phys. Rev. E* **2002**, *65*, 051505.
(9) Roushdy, M. *Mol. Cryst. Liq. Cryst.* **2006**, *457*, 151–160.
(10) Bellini, T.; Clark, N.A.; Muzny, C.D.; Wu, L.; Garland, C.W.; Schaefer, D.W.; Oliver, B.J. *Phys. Rev. Lett.* **1992**, *69*, 788–791.
(11) Leadbetter, A.J.; Richardson, R.M.; Colling, C.N. *J. Phys. France* **1975**, *36*, 37–43.
(12) Bernal, J.D.; Fankuchen, I. *J Gen. Physiology* **1941**, *25*, 111–U8.
(13) Castelletto, V.; Hamley, I.W. *Polym Adv Technol* **2006**, *17*, 137–144.
(14) Alexander, L.E. *X-ray diffraction methods in polymer science*. Wiley: New York, 1969.
(15) de Andrade Lima, L.R.P.; Rey, A.D. *Phys. Rev. E* **2004**, *70*, 011701.
(16) Leadbetter, A.J.; Norris, E.K. *Mol. Phys.* **1979**, *38*, 669–686.
(17) Bras, W.; Emsley, J.W.; Levine, Y.K.; Luckhurst, G.R.; Seddon, J.M.; Timimi, B.A. *J. Chem. Phys.* **2004**, *121*, 4397–4413.
(18) Pereira, F.V.; Borsali, R.; Merlo, A.A.; Da Silveira, N.P. *Liq. Cryst.* **2004**, *31*, 655–661.